

Venus Spherical **Harmonic** Gravity Model to Degree and **Order 60**

ALEX S. KONOPLIV

Jet Propulsion Laboratory, California Institute of Technology

California Institute of Technology

Mail Stop 301-125J

4800 Oak Grove Drive, Pasadena, CA 91109

WILLIAM L. SJOGREN

Jet Propulsion Laboratory, California Institute of Technology

California Institute of Technology

Mail Stop 301-150

4800 Oak Grove Drive., Pasadena, CA 91109

Number of pages: 39

Number of figures: 14

Number of tables: 1

Submitted to Icarus

March 1, 1994

Running head:

VENUS GRAVITY: DEGREE AND ORDER 60

Correspondence:

ALEX S. KONOPLIV

Jet Propulsion Laboratory, California Institute of Technology

California Institute of Technology

Mail Stop 301 -125J

4800 Oak Grove Drive., Pasadena, CA 91109

(818) 354-6105

ask@krait.jpl.nasa.gov

ABSTRACT

The Magellan and Pioneer Venus Orbiter radiometric tracking data sets have been combined to produce a 60th degree and order spherical harmonic gravity field. The Magellan data include the high precision X-band gravity tracking from September 1992 to May 1993 and post-aerobraking data up to January 5, 1994. Gravity models are presented from the application of Kaula's power rule for Venus and an alternative a priori method using surface accelerations. Results are given as freeair surface acceleration, geoid, Bouguer, and isostatic anomaly maps with errors for the freeair and geoid maps included. Correlation of the gravity with topography for the different models is also discussed.

1. INTRODUCTION

On May 25, 1993, the Magellan spacecraft began aerobraking through the atmosphere of Venus to reduce the initial three hour 15 minute orbit to a neat circular 95 minute orbit, This new orbit provides a much greater sensitivity to the gravity in the polar regions than the previous **Magellan** and Pioneer Venus Orbiter (**PVO**) orbits. This has greatly improved the global gravity solution for Venus with more improvements to come as additional tracking is collected.

The initial **Magellan** mapping orbit had a **periapse** altitude of 250 km and an **apoapse** altitude of 8400 km but no direct tracking of **periapse** was available due to the **SAR** imaging of Venus. At the beginning of cycle 4 on Sept 14, 1992 (one cycle is 8 months and provides global longitudinal coverage for the **near polar orbits**), **periapse** was lowered to 170 km and high precision X-band tracking began, **Konopliv et al. (1993)** displayed the initial gravity results with the first four months of cycle 4 data and the better resolution available versus the more eccentric **PVO** orbit and lower quality S-band data, Gravity from **PVO** data had been previously determined by **Mottinger et al. (198 S)**, **Bills et al. (1987)**, **Reasonberg and Goldberg (1992)**, and **Nerem et al. (1993)**. **McNamee et al. (1993)** combined the **PVO** data with the **apoapse** tracking of **Magellan** from the first two cycles.

At the completion of aerobraking on August 6, 1993, cycle 5 data collection began with **periapse** altitude near 180 km and **apoapse** altitude between 500 and 600 km. The gravity solutions presented in this paper include cycle 5 tracking up to January 5, 1994 and show substantial improvement in the gravity in the north polar region and especially that of **Ishtar Terra**, Globally, the 60th degree and order spherical **harmonic** gravity solutions show greater correlation with topography and better **determination** of the **rms** magnitude spectrum.

11. SPACECRAFT TRACKING

The Magellan and PVO spacecraft were tracked with two-way coherent Doppler acquired at the Deep Space Network complexes at Goldstone, California; Madrid, Spain; and Canberra, Australia. The PVO data coverage is the same as described by Konopliv et al. (1993) and McNamee et al. (1993) and includes the recent 1992. data and prior low and high altitude data from 1978 to 1982. The data set basically provides multiple global longitudinal coverage for a narrow latitude band ($\pm 20^\circ$) about the periaipse latitude of 14°N due to the highly eccentric ($e=0.84$) near polar orbit ($i=106^\circ$). The PVO data consist of S-band uplink and downlink with measurement noise typically better than 1 m/s for 60 second compression times. The PVO data, however, is weighted at 3 mm/s for the gravity solutions to give preference to the better Magellan data.

The Magellan tracking data consist of X-band uplink and downlink Doppler data compressed to 10 second intervals, The precision of the X-band measurements typically is better than 0.1 mm/s for 1 minute compression times but is weighted at 0.5 to 2.0 mm/s when processed, During cycle 4, periapsis was near 10°N latitude and provided global longitudinal coverage with a slightly larger latitude band ($\pm 30^\circ$) than PVO due to the smaller eccentricity of Magellan ($i=85.4^\circ, e=0.40$). The data strength for cycle 4 is generally uniform except for degradation between 20°W and 0° longitude due to a near face-on orbit geometry. Cycle 5 began with periapse occulted at 90°E longitude but with apoapse tracking available at 540 km altitude at 90°W . Periapse longitude progressed eastward at 1.5° per day until periapse was visible at 220°E on November 1, 1993. Thus apoapse was visible to about 60°E before occultation but the data quality degraded slightly with time due to an increase in apoapse altitude (see Figure 1) and the face-on geometry. Periapse tracking continued to January 5, 1994 (55°W) at which time the data quality became very poor because of solar conjunction. Tracking after solar conjunction will be incorporated into future gravity models and should include excellent periapse tracking over Maxwell

Fig
1

Mons and additional **periapse** tracking to April 1, 1994 (90°E) at which time **periapse** is occulted, This will improve the resolution of Alpha **Regio** and the southern highlands of **Lada Terra**,

Both the PVO and **Magellan** data sets were divided up into many data time spans (or arcs) where each arc is dynamically continuous and has a separate solution for spacecraft position and velocity at the epoch. All the available PVO data were processed as in **Konopliv et al, (1993)** with data arc lengths typically seven days long but no more than 10 days long. The PVO data arcs were chosen to be as long as practical given the imperfect knowledge of the spacecraft non-gravitational accelerations. For **Magellan**, the data arc lengths were typically three orbits for cycle 4 data; **Konopliv et al. (1993)** arc lengths were less than one orbit. Only the X-band data were processed from cycle 4 with three orbits (one arc) per day included in the **gravity** solutions. This incorporates the majority but not all the available X-band data from cycle 4 and provides a longitudinal spacing of 1.5° or better between **arcs**. All the data from **cycle 5** is used in the gravity solution due to the difficulty in determining a near circular planetary orbit, This includes X-band **uplink** and **downlink** (this data began August 17, 1993), S-band **uplink** and X-band **downlink**, and S-band **uplink** and **downlink**. The S-band **Magellan** data is weighted at 2 to 4 mm/s. The arc lengths for **cycle 5** are typically one day long (up to 15 orbits) and there is a data arc every day. Unlike cycle 4, cycle 5 data arcs may have gaps of several orbits where the spacecraft was not tracked.

III. GRAVITY ESTIMATION

The PVO and **Magellan** Doppler observations were processed using **JPL**'s Double Precision Orbit Determination Program (**DPODP**) (Moyer, 1971). The **DPODP** estimates the spacecraft state and other parameters using a **square root** information weighted least squares filter (**Bierman, 1977**) in the coordinate system defined by the Earth's mean

equator at the epoch of J2000. The parameters that are estimated consist of arc dependent variables (spacecraft state, etc.) that are determined separately for each data arc and global variables (harmonic coefficients, etc.) that are common to all data arcs. The global parameters are determined with a technique described by Illis (1980) that merges only the global parameter portion of the squareroot information arrays from all the arcs of PVO and Magellan, but is equivalent to solving for the global parameters plus arc dependent parameters of all arcs.

We estimate the following global parameters: the normalized spherical harmonic coefficients $(\bar{C}_{nm}, \bar{S}_{nm})$ of the gravity field to degree and order 60, the gravitational constant times the mass of Venus (GM), and the ephemerides of the Earth and Venus. The spherical harmonic expansion of the gravitational potential U is given by

$$U = \frac{GM}{r} + \frac{GM}{r} \sum_{n=2}^{\infty} \sum_{m=0}^n \left(\frac{a_c}{r}\right)^n P_{nm}(\sin \phi) [C_{nm} \cos m\lambda + S_{nm} \sin m\lambda]$$

where r is the distance from the center of the body, a_c is the mean radius of the body and is equal to 6051 km for our Venus models, P_{nm} are the associated Legendre polynomials, ϕ is the latitude, λ is the longitude, and C_{nm} and S_{nm} are the spherical harmonic coefficients for degree n and order m. The normalized coefficients \bar{C}_{nm} and \bar{S}_{nm} are solved for and are related to the unnormalized coefficients by (Kaula, 1966)

$$(\bar{C}_{nm} \text{ or } \bar{S}_{nm}) = \left[\frac{(n+m)!}{(2-\delta_{0m})(2n+1)(n-m)!} \right]^{1/2} (C_{nm} \text{ or } S_{nm})$$

where δ_{0m} is the Kronecker delta function and $\bar{C}_{n0} = -\bar{J}_n$. The harmonic coefficients of degree one are fixed to zero since the origin of the coordinate system is chosen to be the center of mass of the body. The \bar{J}_2 coefficient is not corrected for the permanent tide and a small bias of 4.0×10^{-9} must be subtracted from our \bar{J}_2 if it is to be compared with McNamee et al. (1993) or Nerem et al. (1993) (Love number $k_2 = .255$). However, this correction is far less than the error in \bar{J}_2 . The total number of global parameters is 3730

including 3717 harmonic coefficients. Brouwer and Clemence (1969) Set III parameters are estimated to obtain the deviation of the Venus relative to the Earth ephemeris from the JPL DE200 planetary ephemeris as determined by Standish (1990). In Konopliv et al, the pole orientation and rotation rate of Venus were estimated, but in this paper they are fixed to the 1991 IAU values which include recent results from Magellan (Davies et al, 1992).

The at-c dependent parameters that are estimated in the general order of their importance are the atmospheric density, velocity deltas from momentum wheel desaturations (Magellan only), solar radiation pressure coefficients in three orthogonal directions, small velocity deltas for star calibrations (Magellan only), apoapse residual velocity deltas per day for PVO (less than 1 mm/s) to account for unmodeled nonconservative forces, acceleration vectors for spacecraft orientation changes to heat or cool down the Magellan spacecraft (“hides”), and an Earth rotation (UT1) bias for the PVO arcs. The desaturations for Magellan occur for every orbit in cycle 4 and cycle 5 and thus 3 velocity vectors were solved for in cycle 4 arcs and up to 15 velocity vectors were solved for in cycle 5 arcs with magnitudes generally less than 1mm/s. Additional dynamic models include gravitation of the planets and Sun (using JPL DE200 masses and ephemerides), relativistic terms due to Venus and the Sun, and Venus albedo forces on the spacecraft.

For atmospheric drag, the Venus international Reference Atmosphere (VIRA) model is used, It is a multi-layered model with density values at 5 km intervals in altitude and profiles given at different local solar times (Keating et al., 1985). The exponential scale- height values for each layer are held fixed and the density at the lowest layer of 140 km is estimated for each passage through the atmosphere. For periapsis altitudes above 250 km (including the 1000 km altitude PVO data), a single-layered atmosphere is used with scale- height values remaining a function of local solar time.

For the Doppler observable, averaged seasonal troposphere calibrations were applied (Chao, 1972) and ionosphere corrections are additionally applied to the Magellan X-band observable. Any observations below 10° elevation were deleted because of

unmodeled troposphere effects. Daily UT1 and polar motion values from JPL Space91 solution (Gross, 1992) were used for data prior to 1983 and otherwise values produced by the University of Texas at Austin (also submitted to International Earth Rotation Service) were used. Station locations produced by Folkner (1992) with appropriate precession and nutation, solid-earth tide, and plate motion models were used.

Once the global portion of the information arrays from all the PVO and Magellan data arcs are combined, an a priori constraint is applied to the harmonic coefficients. This constraint is needed due to the lack of uniform global measurements of the gravity field. Otherwise, the coefficients would take on unrealistic values and the surface gravity signatures would be highly artificial ("aliased") where the data is weak. The common practice is to constrain each coefficient to zero with an uncertainty given by the Kaula rule (1966) with mass adjustments for that particular planet (used in Konopliv, 1993, Nerem 1993, McNamee 1993). For Venus, the Kaula rule used is $1.2 \times 10^{-5}/n^2$ where n is the degree of the coefficient.

The alternative method is to constrain the surface gravity directly to avoid aliasing without constraining the individual coefficients, and hence avoids a global suppression of the power spectrum. To choose the surface areas for constraint, we map the unconstrained gravity covariance to the surface of Venus (i.e., the mean surface of 6051 km), and any areas with uncertainties greater than 40 milligals we constrain with surface measurements. The surface measurements are artificial radial surface accelerations generated from the Kaula constrained solution at intervals of two degrees and with an uncertainty of 20 milligals. Thus, Kaula's rule is in the constraint, but indirectly. In addition, four surface areas are slightly constrained at 40 milligals or greater due to the appearance of possible aliasing. They are the north pole (86° to 88°) because of the hole at the pole from the Magellan orbit inclination, the area just south of Themis Regio, the area northeast of Maxwell Mons, and the area northeast of Atla Regio. There is flexibility in the method for choosing the surface constraints and we have found comparable results for different cutoffs

of the surface covariance. We will attempt to fine tune future models. However these changes are small compared to the difference between the surface acceleration a priori (SAAP) models and the Kaula constrained solutions. This method is similar to the current method being used for the determination of the Earth's gravity field (the JGM models, Nerem 1994). Prior Earth gravity models used the Kaula rule as the constraint.

IV. GRAVITY RESULTS

The gravity solution for this article is named MGNP60FSAAP (Magellan plus IWO, 60th degree and order, F series with surface acceleration a priori) and will be compared to the best solution available with the Kaula constraint (MGNP60F). There is a slight difference in the data weights for the solutions (cycle 5 data is deweighted from 1 mm/s to 2 mm/s for MGNP60F), but comparisons would be similar even if the data weights for the Kaula solution were the same as the SAAP solution. For future SAAP gravity fields, we might be able to weight the data even closer to the actual noise and hence avoid the deweighting of data that is typically done for Kaula constrained solutions.

The surface accelerations and geoid for MGNP60FSAAP are displayed in Figures 2 and 3. The resolution at periapse (such as Bell Regio) is comparable to previous results where there was cycle 4 data (Konopliv, et al., 1993) but the resolution over Ishtar Terra is greatly improved due to the lower spacecraft altitude (1000 km for cycle 4 versus 400 km for cycle 5). The mountains surrounding the plateau are beginning to be resolved and the amplitude of Maxwell Montes has increased from 135 milligals to 180 milligals. The amplitude for Freyia Montes is 100 milligals and for Akna Montes is 80 milligals. It is now possible to place these highland terrains in approximately the same category as Aphrodite Terra, which apparently has undergone considerable relaxation and is not at all a feature similar to Atla Regio or Beta Regio. In the southern hemisphere, the peaks of Lada Terra such as Quetzalpetlatl are being resolved that were questionable in previous results. Other

Figure
2 ,

unnamed topographic highs (1 18°W,600S and 70 °W,700S) also show as positive gravity anomalies.

Figure 4 displays the freeair acceleration uncertainty from the covariance prior to constraining the harmonic coefficients with surface acceleration measurements. Any surface in Figure 4 with errors greater than 40 milligals is constrained with artificial surface measurements, The four small surfaces that are also constrained have unconstrained errors in Figure 4 between 20 and 40 milligals. Without the cycle 5 data, the unconstrained errors are far greater than 1000 milligals for latitudes above 50°N and below 30°S. With the surface constraints, the freeair acceleration uncertainty and geoid error are displayed in Figures 5 and 6. The uncertainties in the regions that are constrained are optimistic but these regions will diminish in size as additional Magellan data is incorporated into the solution. The errors near periapse are fairly realistic if not conservative and are about 6 milligals for the accelerations and one meter for the geoid.

Figures 7 and 8 display the “rms magnitude spectrum of the gravity fields. Let \underline{G}_n be the vector of all gravity coefficients for degree n, then the spectrum is given by $G_n/(2n+1)^{1/2}$ where G_n is the magnitude of \underline{G}_n . In Figure 7, the Kaula rule for Venus is given along with the spectrum and uncertainties for the constrained MGNP60FSAAP solution and an unconstrained solution (no a priori on the coefficients). The surface constrained solution (MGNP60FSAAP) shows considerable more power in the higher degrees versus the Kaula constrained solution (MGNP60F). The covariance for MGNP60FSAAP indicates the spectrum is determined to degree 40 but this is probably optimistic. However, from the no a priori solution, we conclude the spectrum is determined to at least degree 25 versus degree 17 from previous results (Konopliv et al., 1993). Figure 8 compares our solution with previous results and shows increased power over the preliminary cycle 4 solution PMGN60C (Konopliv et al., 1993) and PVO only solutions (as given by Nerem et al., 1993). It should be mentioned that along with the increased

Figure
4

Figures
5, 6

Figures
7, 8

power, the SAAP solution only increased the root sum of square of the residuals (RSOS) by 0.96% versus a 3.77% increase from applying a Kaula constraint.

The MGNP60FSAAP coefficients truncated to degree and order 21 and formal errors are given in Table 1 (the full field can be requested from the author using the E-mail address ask@krait.jpl.nasa.gov or obtained from the Planetary Data Node at Washington Univ., St. Louis, Me.). The GM solution and formal error for MGNP60FSAAP is 324858.628Ml.016 and agrees well with the previous results of Konopliv et al, (1993) and Nerem et al. (1993). The principal axes of inertia are determined from the second degree coefficients and for MGNP60FSAAP, the latitudes and longitudes are (1) O. 19°N, 2.89°W, (2) 0.42°N, 87.11 °E, and (3) 89.54°N±0.05°, 117.27°W. With the formal error of 0.05°, the polar principal axis still shows an offset from the rotational axis and may indicate a wobble (Yoder and Ward, 1979), although confidence in this result must be demonstrated by additional Magellan data and higher degree and order solutions.

Figure 1 shows the Magellan cycle 5 actual orbit history along with predictions for about 100 days for MGNP60FSAAP and the gravity field (VGM6A) from McNamee et al. (1993) which is based upon Magellan data prior to cycle 4 and is representative of the accuracies available from pre-aerobraking gravity fields. The propagation begins October 1, 1993 (56 days after August 6 when aerobraking ends) and is a few days after a periapse raise maneuver. For the MGNP60FSAAP model, the 1-km error in periapse and 5-km error in apoapse altitude after 100 days is a combination of comparable errors in the gravity, atmospheric drag (or VIRAModel which can have errors of 50% in density), and small delta velocities from the momentum wheel desaturations. The propagation is insensitive to errors in the initial spacecraft position and velocity. Figure 9 shows a global longitude test for cycle 1,2, and 3 data with the same modeling assumptions as McNamee et al. (1993). It displays the rms of the X-band data for one-day solutions (8 orbits with one density parameter estimated) and shows the improvement of MGNP60FSAAP versus VGM6A of McNamee et al. (1993). The VGM6A solution basically has this data included

Table 1

Figure 9

in the field and the **MGNP60FSAAP** solution has cycle 4 data at a slightly lower periapse altitude (170-km versus 250 km) but with shorter arcs and more momentum wheel desaturations. The increase in rms from 60°E to 90°E longitude is mostly from gravity, and improvement should occur from additional cycle 5 data to April 1, 1994 when periapse is occulted at 90°E longitude. The remaining rms in Figure 9 is mostly from modeling errors other than the gravity and measurement noise.

The correlation with topography for the **MGNP60FSAAP** model is given in Figure 10. With \mathbf{T}_n being the vector of all topography coefficients for degree n, the correlation for degree n is given by $\gamma_n = (\mathbf{G}_n \cdot \mathbf{T}_n) / (G_n T_n)$. The topography coefficients are a 60th degree and order truncation of a 360th degree and order topography solution by Rappaport (1994, solutions can be requested at E-mail address njb@nomad.jpl.nasa.gov). This is an improved solution using a finer grid of topography data versus the 120 degree and order solution of Konopliv et al. (1993), Both solutions used PVO, Venera, and Magellan topography data with the Magellan data from Ford and Pettengill et al. (1992). The correlation error bars are determined from the full gravity covariance with the assumption that the errors in the topography coefficients are negligible compared to the gravity. The new topography, however, shows noticeably greater correlations with gravity. If this is an indication of the error in the topography coefficients, then the correlation errors are dominated by the error in the topography coefficients up to degree 30 and are dominated by gravity errors for degrees higher than 30. The correlation errors are probably realistic beyond degree 30 and the correlations are most likely lower than the true values since the correlations continue to increase as more Magellan data is added to the gravity solution. Figure 11 compares the correlation with topography for different solutions. Note the substantial increase in correlations for the new Magellan and PVO based solutions versus the PVO only solutions, and the increase in the correlations especially in the higher degrees for the SAAP solution versus the Kaula rule solution.

Figure 12 displays the Bouguer anomalies for the surface of Venus and is the difference between the MGNP60/SAAP accelerations and the theoretical acceleration from uncompensated topography. A mean density of 5.248 g/cm^3 and surface density of 2.9 g/cm^3 were used. This map is an indication of compensation depth with large negative anomalies indicating relatively shallow compensation such as Ishtar, Maxwell Mons, Thetis, and Ovda. The smaller values values such as Atla and Beta Regio point to deeper compensation or possible areas with dynamic support. Another method of analyzing compensation is to map the isostatic anomalies. The admittance function for each degree n is given by $F_n = \gamma_n(G_n/T_n)$ and is displayed in Figure 13 along with the theoretical Airy type compensation depth (see Mottinger et al, 1985). Since F_n is equal to the correlation times the ratio of rms magnitude spectrums, the error in the admittance function is similar to the error in the correlation. As more Magellan data is added to the gravity field, the correlations with topography are expected to increase especially in the higher degrees (40-60) and the power in the gravity rms spectrum will slightly increase. This will increase the admittance function in the higher degrees but not more than double (i.e. compensation depths have an upper bound of 50 km). Thus assuming Airy compensation for the shorter wavelength features (degrees 30 to 60), the Moho depth is between 25 and 50 km. The vector of coefficients for degree n for the isostatic anomalies are calculated as $I_n = G_n - F_n T_n$. Figure 14 displays the isostatic anomalies and indicate the depth of compensation with respect to a global average per degree (the isostatic coefficients were truncated at degree 55 since some aliasing appears from higher order effects). So again, the regional compensation for areas such as Beta and Atla are deeper than the global average and areas such as Ovda and Maxwell are more shallow than global averages.

Figure
12

Figure
13

Figure
14

v. CONCLUSIONS

The **MGNP60FSAAP** gravity solution represents our best spherical harmonic gravity solution to date, It shows substantially higher correlations with topography versus previous results and especially better resolution near **Ishtar** Terra, The method of artificial surface accelerations used to constrain the solution shows more promise than direct application of the **Kaula** power rule. **Postfit** residuals are noticeably lower and increased correlations with topography are visibly demonstrated by improved resolution at **periapse**. However, postfit residuals indicate perturbations greater than degree 60 are present and future models may be solved to a higher degree.

ACKNOWLEDGMENTS

We would like to thank the JPL Magellan Navigation Team (K. Wong and T-H You), Gene Goltz, Jeff Plaut, Nicole Rappaport, and Eric Graat of the Jet Propulsion Laboratory and Algis Kucinskas at Cornell University for help in processing and analyzing the Magellan data. The research described in this paper was carried out by the Jet Propulsion Laboratory, California Institute of Technology, under a contract with the National Aeronautics and Space Administration.

REFERENCES

- BIERMAN, G.J. (1977). *Factorization Methods for Discrete Sequential Estimation*. Academic Press, New York.
- BILLS, B. G., W.S.KIEFFER, and R.L. JONES (1987) Venus Gravity: A Harmonic Analysis. *J. Geophys. Res.* 92, 10335-10351.
- BROUWER, D. and G. CLEMENCE (1961). *Methods of Celestial Mechanics*. Academic Press, New York, 241.
- CHAO, C. C. (1972). The Tropospheric Calibration Model for Mariner Mars 1971. TR 32-1587, JPL Internal Document, Jet Propulsion Laboratory, Pasadena, CA.
- DAVIES, M. E., V.K. ABALAKIN, A. BRAHIC, M. BURSA, B.H.CHOVITZ, J.H. LIESKE, P.K. SEIDELMANN, A.T.SINCLAIR, and Y.S. TJUFLIN (1992). Report of the IAU/IAG/COSPAR Working Group on Cartographic Coordinates and Rotational Elements of the Planets and Satellites: 1991. *Celest. Mech.*, 53, 377-397.
- ELLIS, J. (1980). Large scale state estimation algorithms for DSN tracking station location determination. *J. Astronaut. Sci.* 28, 15--30.
- FOLKNER, W. M., C. S. JACOBS, O. J. SOVERS (1991). Radio Source Catalog for the Mars Observer Project, IOM 335. 1-91-034, JPL Internal Document, Jet Propulsion Laboratory, Pasadena, CA.
- FORD, P.G. and G.H.PETTENGILL (1992). Venus Topography and Kilometer-Scale Slopes. *J. Geophys. Res.*, 97, 13103-13114.
- GROSS, R.S. (1992). A Combination of Earth Orientation Data: Space91. In *IERS Technical Note 11, Earth orientation reference frames and atmospheric excitation functions submitted for the 1991 IERS Annual Report* (P. Charlot, Ed.),. IERS, Paris, France.

- KAULA, W. M. (1966). *Theory of Satellite Geodesy*. Blaisdell Publishing Company, Waltham, Massachusetts.
- KEATING, G. M., J. L. BERTAUX, S. W. BOUGHER, T. E. CRAVENS, R. E. DICKENSON, A. E. HEDIN, V. A. KRASNOPOLSKY, A. F. NAGY, J. Y. NICHOLSON III, L. J. PAXTON, U. VON ZAHN (1985). Models of Venus Neutral Upper Atmosphere: Structure and Composition. *Adv. Space Res. S*, 117-171.
- KONOPLIV, A. S., N.J. BORDERIES, P.W. CHODAS, E.J. CHRISTENSEN, W.L. SJOGREN and B.G. WILLIAMS (1993), Venus Gravity and Topography: 60th Degree and Order Model. *Geophys. Res. Lett.* 20,2403-2406.
- MCNAMEE, J. B., N.J. BORDERIES and W.L. SJOGREN (1993), Venus: Global Gravity and Topography. *J. Geophys. Res. Planets* 98,9113-9128.
- MOTTINGER, N. A., W. I., SJOGREN and B.G. BILLS (1985). Venus Gravity: A Harmonic Analysis and Geophysical Implications. *J. Geophys. Res.* 90,739-756.
- MOYER, T. D. (1971). Mathematical Formulation of the Double-Precision Orbit Determination Program (DPODP). Technical Report 32-1527. JPL internal document, Jet Propulsion Laboratory, California Institute of Technology, Pasadena, CA.
- NEREM, R. S., B.G. BILLS and J.B. MCNAMEE (1993). A High Resolution Gravity Model for Venus: GVM-1. *Geophys. Res. Lett.* 20, 599-602.
- NEREM, R. S., F.J. LERCH, J.A. MARSHALL, E.C. PAVLIS, B.H. PUTNEY, J.C. CHAN, S.M. KLOSKO, S.B. LUTHCKE, G.B. PATEL, N.K. PAVLIS, R.G. WILLIAMSON, B.D. TAPLEY, R.J. EANES, J.C. RIES, B.E. SCHUTZ, C.K. SHUM, M.M. WATKINS, R.H. RAPP, R. BIANCALE, and F. NOUEL (1994). Gravity Model Development for TOPEX/Poseidon: Joint Gravity Model-1 and 2, submitted to *J. Geophys. Res.*
- RAPPAPORT, N.J. (1994). Private communication.
- REASENBERG, R.D. and Z.M. GOLDBERG (1992). High-Resolution Gravity Model of Venus. *J. Geophys. Res.* 97, 14681-14690.

- STANDISH, E. M, (1990). The observational basis for JPL's DE200, the planetary ephemeris of the Astronomical Almanac. *Astron. Astrophys.* 233, 252-271.
- YODER, C.F., and W.R. WARD (1979). Does Venus Wobble? *Astrophys. J.* 233, 33-37.

Table 1. Normalized Harmonic Coefficients and formal errors ($\times 10^{10}$) for MGNP60FSAAP up to degree and order 21 ($\bar{C}_{n0} = \bar{J}_n$).

n	m	C_{nm}	S_{nm}	c_{nm}	$\sigma_{S_{nm}}$						
10	7	-1613.1	--/46.5	11.1	10.0						
10	8	1341.5	1138.3	10.1	1.8						
10	9	1-146.8	-829.4	9.7	8.-/						
10	10	-458.3	172.9	17.8	9.4						
11	0	505.6	.0	30.6	.0						
11	1	-2344.9	-755.7	33.4	26.7						
11	2	10-/6.8	3*15.5	26.1	28.5						
11	3	1068.-/	-1239.4	25.1	23.6						
11	4	-120.4	1749.0	21.2	21.4						
11	5	-120.9	214.9	17.9	18.1						
11	6	-80.5	144).5	15.1	14.4						
11	7	-55.?	-1105.1	12.2	11.9						
11	8	395.?	360.5	10.7	10.2						
11	9	6*/.?	8-/1.0	8.1	8.3						
11	10	368.0	?36.0	9.1	9.4						
11	11	1299.6	-1223.6	9.1	9.3						
12	0	-369.6	.0	33.0	.0						
12	1	151.4	-814.9	35.6	29.1						
12	2	1321.9	-)50.4	28.2	31.4						
12	3	--/81.8	-536.8	2-/2	26.0						
12	4	646.3	319.4	23.5	23.3						
12	5	1821.1	-1918.9	20.3	20.-/						
12	6	1348.3	902.7	18.0	17.5						
12	7	1063.7	-435.9	14.9	14.7						
12	8	-1055.1	93.8	12.6	12.5						
12	9	-578.2	-30.8	10.3	10.4						
12	10	1785.4	-333.9	9.5	8.8						
12	11	874.1	-2304.6	9.0	9.1						
12	12	-158-/2	-484.6	11.2	11.4						
13	0	-1681.1	.0	35.3	.0						
13	1	-318.3	-578.5	38.6	31.1						
13	2	386.6	-1103.8	30.6	34.1						
13	3	1020.4	-659.2	29.7	28.6						
13	4	-117/.4	-10-/5.9	26.3	26.7						
13	5	1011.5	-1249.9	22.-/	23.1						
13	6	-492.)	508.0	20.3	20.3						
13	7	-53.0	1105.9	17.4	17.4						
13	8	-64.4	441.2	14.4	14.7						
13	9	120.6	1792.4	11.9	12.2						
13	10	369.3	-420.3	10.1	10.6						
13	11	-1111.2	-584.3	8.3	8.4						
13	12	-658.6	-2-/4.-/	9.0	9.0						
13	13	858.6	351.1	8.3	8.3						
14	0	-213.9	.0	37.1	.0						
14	1	-542'.0	-1319.2	39.5	31.6						
14	2	588.9	-294.3	33.2	35.8						
14	3	1515.5	-605.7	32.2	30.7						
14	4	793.0	-147.6	28.1	28.2						
14	5	-136.9	-8.5	25.2	26.0						
14	6	169.8	-658.6	22.6	22.5						
14	7	-327.4	-540.1	19.8	20.2						
14	8	91.9	-812.4	17.2	17.5						
14	9	-196.6	-718.4	14.6	14.8						
14	10	-76.9	198.5	12.5	12.5						
14	11	-1200.6	-703.8	10.4	10.4						
14	12	-929.8	4*/2,3	9.4	9.4						
14	13	-421.1	-426.6	8.4	8.6						
14	14	-413.8	-1260.0	10.0	9.9						
15	0	-687.6	.0	39.4	.0						
15	1	170.1	670.0	42.1	34.6						
15	2	444.4	-829.9	35.0	38.7						

15 3	-1-/3.3	446.8	34.5	33.5	19 5	345.1	227.9	35.9	35.4
15 4	443.1	-824.9	31.1	31.7	19 6	283. ?	528.9	34,5	33,1
15 5	87.3	7?9.7	?-1.6	28.1	19 7	-157,8	-353.1	31.4	30.1
15 6	-318.2	556.5	?5.7	?5,7	19 8	341,"/	-315.9	30.4	28.6
15 -1	399.2	-173.8	22.4	2?. 7	19 9	-3?5,1	403.4	?6.8	26.2
15 8	598.3	-12.9	19.5	?0,0	19 10	149.0	-35?.4	25,3	24. ?
15 9	-694.8	265.2	1-/.1	17,6	19 11	589.0	-131.6	2?.8	2?.3
15 10	-436.4	694,8	14.2	14.6	19 12	184.5	-78.5	19,7	18.9
15 11	104.1	-46.0	12.3	12.2	19 13	330.6	-595.5	17.6	17,6
15 1?	14.4	-39.7	10.4	10.6	19 14	-163,7	-166.8	14.8	14,6
15 13	481.4	-192.9	8.3	8.3	19 15	235. ?	258.5	1?.8	1?.4
15 14	69.5	102.1	8.5	8.3	19 16	-230,8	-438,2	10.5	10.6
15 15	76. ?	--13.1	7.7	-1.7	19 17	-311 -)	183. "/	8.3	8.4
16 0	51.2	.0	40.7	.0	19 18	389.1	202.0	7.8	7.8
16 1	-516.9	9?0. 6	43.4	35, ?	19 19	544.8	-62.2	6.8	-/.0
16 2	-319.1	733.4	3-1.0	39.1	?0 o	171.2	.0	45.0	.0
16 3	328.9	464.2	36.4	34.7	20 1	??5.1	509.7	48.4	31.7
16 4	676.6	821.5	3?.7	32.6	20 2	45.)	-305.4	42.5	40.4
16 5	-1005.9	3?3.3	30.2	30.5	20 3	-152,4	-346.9	42. -1	39.0
16 6	?33.5	532.1	27.5	?-/.0	20 4	-118.3	-329.5	39.8	35.7
16 "r	151.0	10?7.4	25.4	?5.5	?0 5	-388.7	4?.0	37.7	36.9
16 8	21,3	-148.8	22.0	22.1	20 6	44.2	3-/0.6	35.8	33. ?
16 9	-2?0.8	-857,6	19.6	20.1	20 7	-112,1	-189. ?	34,1	?9.0
16 10	90.4	151.0	1-/. ?	17.4	?0 8	-136.0	570.9	31.3	?3.8
16 11	330.6	61.4	14.8	14.5	20 9	57,2	545.7	30.4	26.8
16 1?	539.0	-268.1	1?.6	1?.6	20 10	-3-1?.3	-1-/3.0	27.1	21.5
16 13	806.0	'/14.8	10.4	10.5	?0 11	-5-/.2'	-63.1	26.0	23.3
16 14	89-1.0	155.6	9.2	9.1	20 12	-19.0	--/1.3	22.7	20.8
16 15	112,1	-41-/. ?	8.2	8.0	20 13	336,3	61.3	20. ?	20.1
16 16	-.?68,0	-1176.5	8,9	8.9	20 14	-185.5	-.3	1-/. -/	17.7
1-/ o	-20-/4	.0	42.4	.0	?0 15	227,6	145.5	15.3	14.8
17 1	-608.3	-499,1	45.1	37.1	20 16	-56.4	65.5	12.8	1?.9
17 2	102,2	897. ?	38. '/	41.5	20 17	-354.9	448.2	10. "/	10,6
17 3	-60-/4	272.7	38.1	3?/.1	20 18	243.1	881.3	8.9	8.9
17 4	-363.0	-389.9	34,9	35.6	20 19	170.0	-406.2	7,6	7.-1
17 5	440.5	-750.3	3?.0	32.4	20 20	29,4	-234.4	7.6	7.6
17 6	-38.7	639.8	30.5	30.4	21 0	371.3	.0	45.9	.0
17 7	205.2	530.3	?-1.1	27.0	21 1	?03.0	-48.8	49.6	41.4
17 8	-433.9	-69.4	?4.9	?5.3	21 2	54.4	-285.7	43.4	46.0
17 9	534.1	218.7	21. ?	22.5	21 3	45.6	3?1 .6	43,9	4?.1
17 10	109.4	793.5	19.3	19.6	21 4	-262,1	90.7	41.1	40. -/
17 11	-510. -/	538.4	17.3	1-/0	21 5	165.6	221.7	38.8	38.5
17 1?	-622,3	-24.6	14.5	14.5	21 6	-1?8.5	501.1	3-/5	36.5
17 13	43?.6	517.3	12.4	12.4	21 "1	-223.4	50.2	34.9	34.0
17 14	584.5	-210.1	10.6	10.3	21 8	1?9.7	-35.2	33.9	3?.1
17 15	5?-1.5	-1573.8	8.5	8.?	21 9	490.0	8.2	30,9	30.1
1"/ 16	?-/4.0	-262.1	"/.9	8.1	21 10	99. "/	8-/3	30.1	?8.8
17 17	-79"1.7	-21.4	7.2	"/.3	21 11	-2?1 .1	144.6	2-/3	26.0
18 0	-349.4	.0	43.5	.0	21 12	-6.4	23.9	25.6	24.6
18 1	15.7	-1?0.9	46.4	38.6	21 13	1?.4	161.1	2?.8	?3.0
18 2	13.3	-30\$3	40.0	43.0	21 14	-534.2	155.1	19.8	19,9
18 3	17.1	-118.7	39.8	38.9	21 15	-177.8	-196.8	18.2	17.6
18 4	458.6	-219.4	36.5	36.9	21 16	183.8	-68.4	14.9	15.0
18 5	-93.0	277.9	34.5	34.8	21 17	-594.1	265.3	1?.8	1?.9
18 6	707.4	3-1?.1	31.8	31.4	21 18	164.1	90.2	10. -1	10.7
18 7	-10.0	797.9	30.4	30.0	?1 19	668.6	-27.8	8,4	8.5
18 8	45.1	647.1	?7.0	26.9	21 20	112,0	-37.5	7.6	-/,7
18 9	-315.3	420.6	25.0	25.4	21 21	352.1	-3?3.6	6.7	6.8
18 10	-86.2	-449.0	2?.3	??.6					
18 11	229.8	17-/8	20.0	19. -/					
18 12	31.9	815,4	17.5	17.4					
18 13	-160.3	369.4	14.8	14.9					
18 14	-19. ?	-683.1	12.8	12.7					
18 15	109.9	-256.8	10. -1	10.3					
18 16	-?64.2	-136.6	9.0	8.9					
18 17	-51.4	-80, -/	7.8	7.8					
18 18	211.4	-213.0	8.2	8.1					
19 0	158.5	.0	44.2	.0					
19 1	518,2	33.9	48.0	39.9					
19 2	-141.5	-306.1	41.2	43.6					
19 3	-308.0	79.1	41.6	40.0					
19 4	-532.6	-?84.4	38.2	38.0					

FIGURE CAPTIONS

FIG. 1. (a-b) History of the Magellan cycle 5 orbit from August 6, 1993 to January 5, 1994 (actual) and gravity field propagations from October 1, 1993 for our gravity field (MGNP60FSAAP) and that of McNamee (VGM6A, 1993). Orbit characteristics displayed are: (a) periapse altitude, (b) apoapse altitude, and (c) periapse latitude. There was a periapse raise maneuver on September 28, 1993.

FIG. 2. Free-air gravity accelerations at the surface of Venus in 20 milligal contour intervals from gravity model MGNP60FSAAP. Negative gravity is displayed with dashed contours,

FIG. 3. Geoid of Venus from MGNP60FSAAP gravity model displayed in 10 meter contour intervals.

FIG. 4. Freeair acceleration error at the surface of Venus in 20 milligal contour intervals for the unconstrained gravity covariance used in the determination of the constraint for the MGNP60FSAAP solution. The contours up to 600 milligals are plotted and the region from 80°E to 210°E in the southern hemisphere has errors of 3000 plus milligals.

FIG. 5. Freeair acceleration error at the surface of Venus in 2 milligal contour intervals for the MGNP60FSAAP solution.

FIG. 6. Geoid errors of Venus in 0.5 meter contour intervals for the MGNP60FSAAP solution.

FIG. 7. Harmonic rms spectrums and uncertainties for the surface constrained solution and unconstrained solution (no apriori on the harmonic coefficients). The spectrum for the solution constrained by the Kaula rule is also given (MGNP60F).

FIG. 8. Comparison of the harmonic rms spectrum of this papers gravity solution with previous results as given by Konopliv et al. (1993, PMGN60C) and Nerem et al. (1993, PVO).

FIG. 9. Comparison of the X-band rms for one-day long solutions for MGNP60FSAAP and VGM6A of McNamee et al. (1993).

FIG. 10. Correlation with topography and error bars for gravity model MGNP60FSAAP.

FIG. 11. Comparison of correlation with topography for (a) MGNP60FSAAP, (b) the Kaula rule solution MGNP60F, (c) preliminary results from cycle 4 as given by Konopliv et al. (1993,PMGN60C), and (d) PVO gravity solution of Nerem et al. (1993).

FIG. 12. Bouguer anomalies at the surface of Venus with 50 milligal contour intervals.

FIG. 13. Admittance function and theoretical compensation depths.

FIG. 14. Isostatic anomalies at the surface of Venus with 10 milligal contour intervals.

Figure 1 (a)
Konopliv

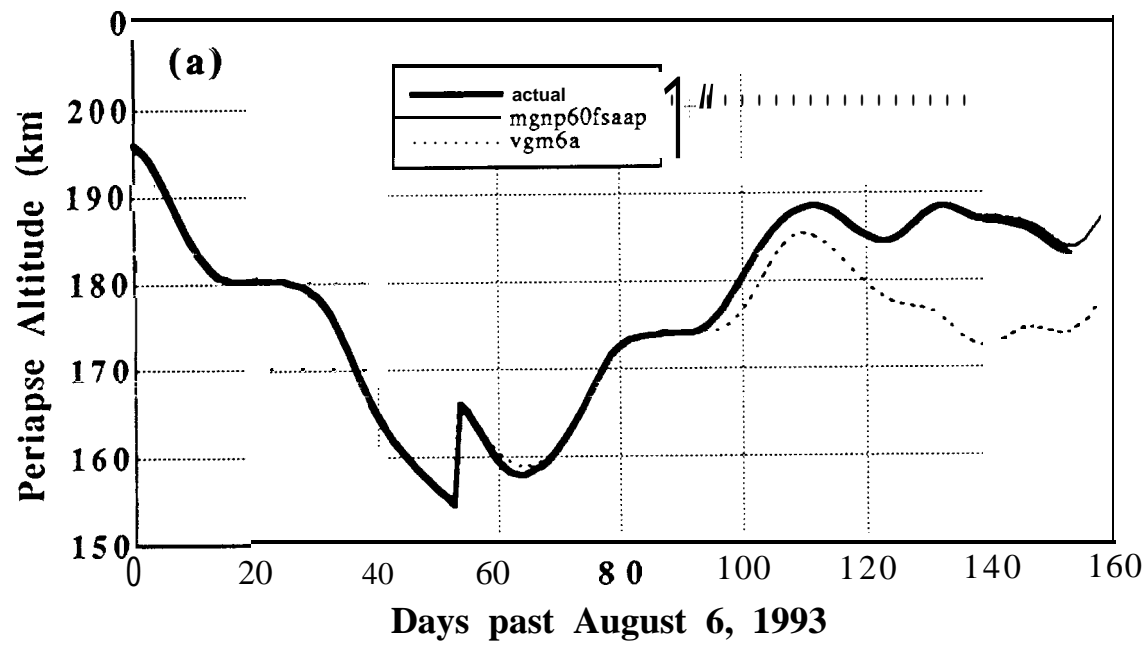


Figure 1 (b)
Komopliv

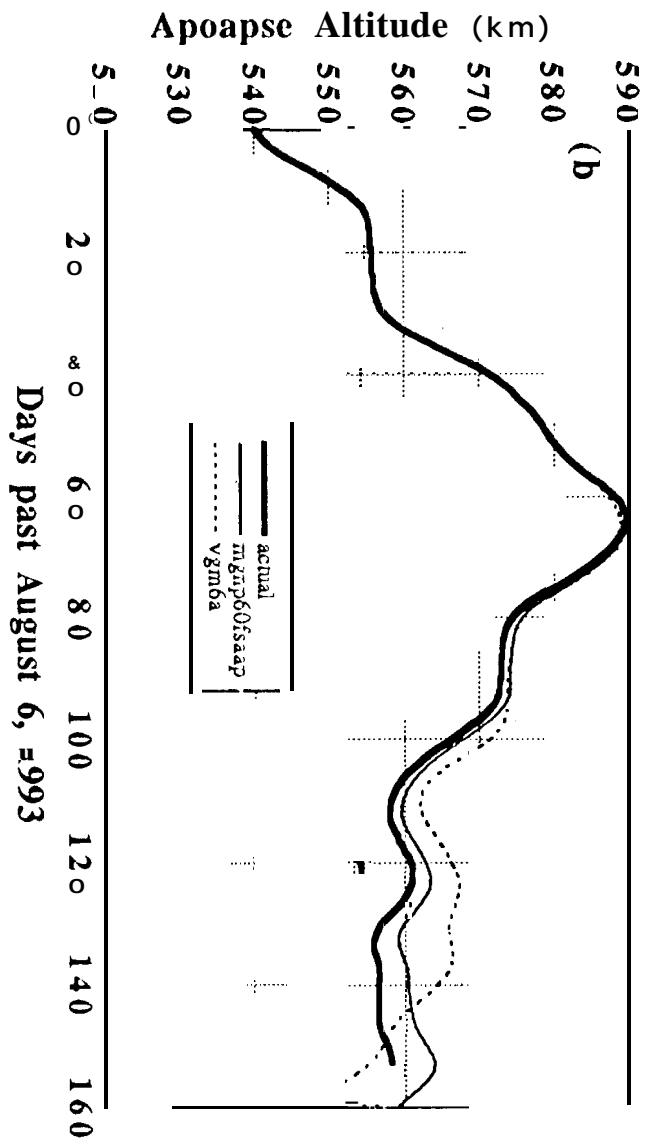


Figure 1 (c)
Kamogiv

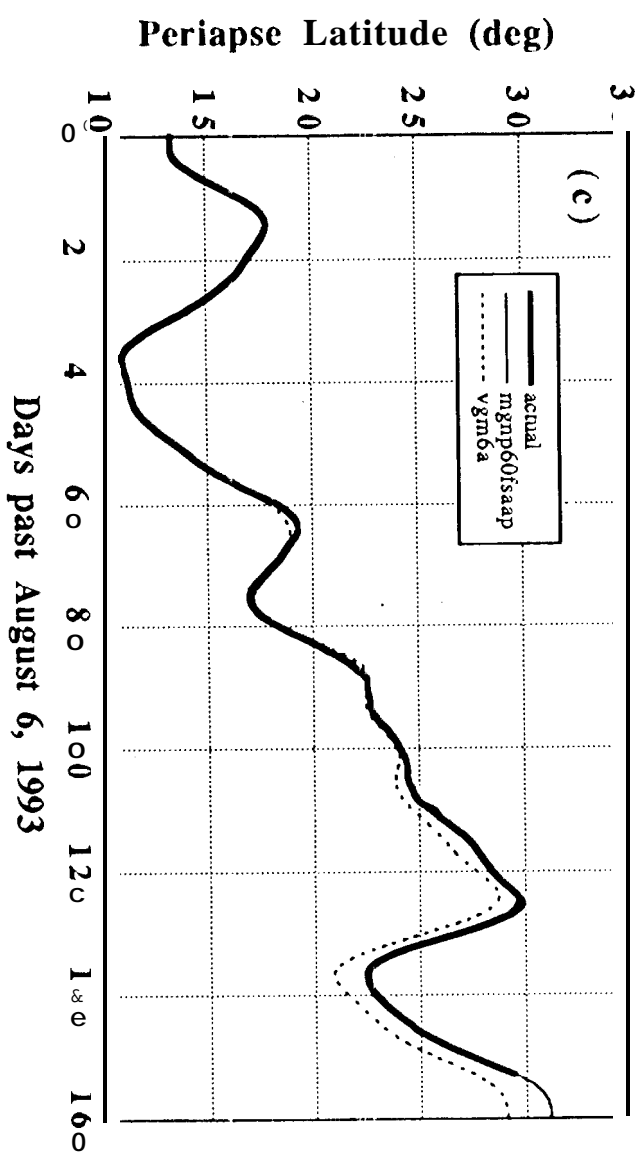
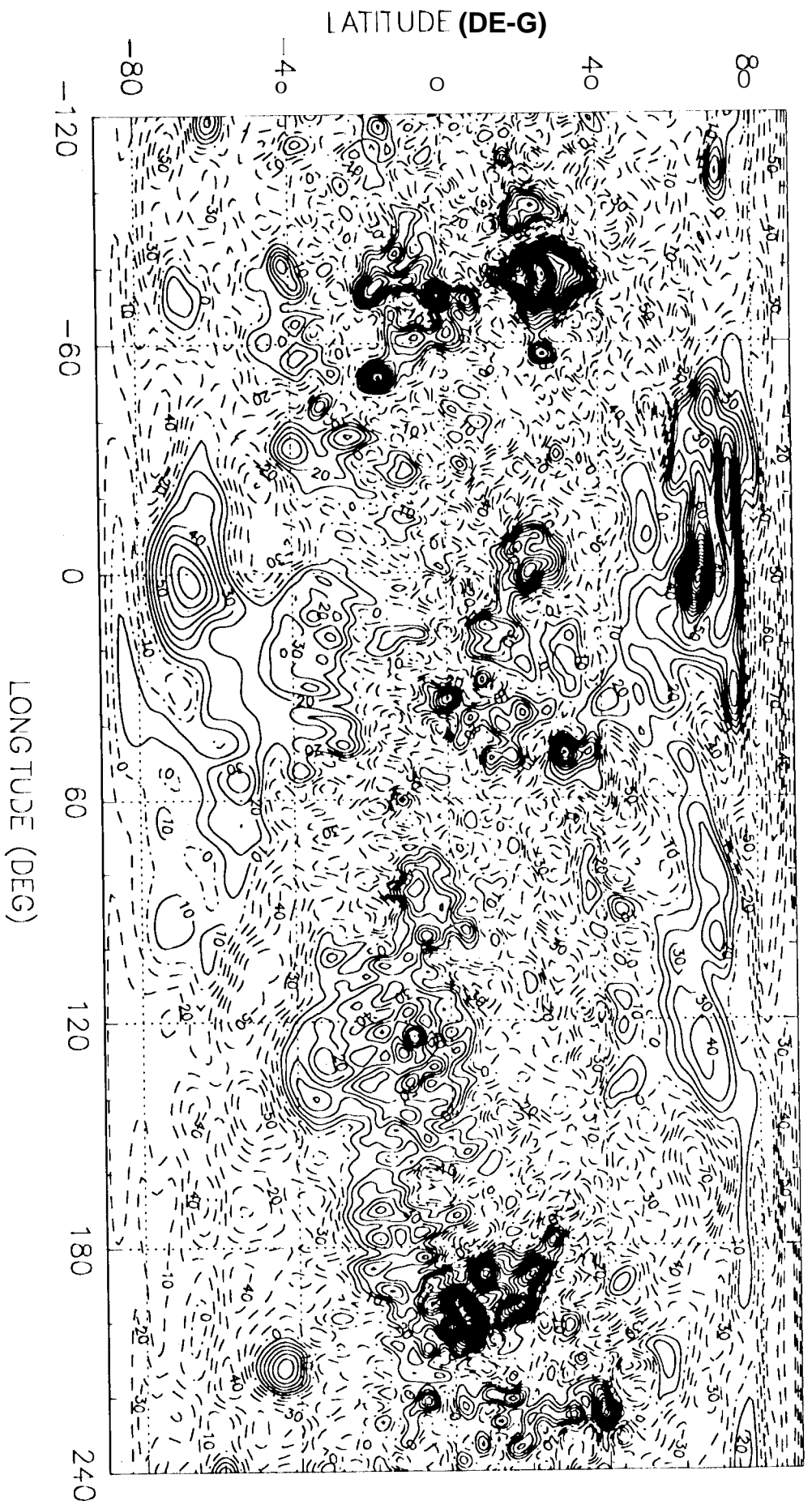


Figure 2
Kovachik



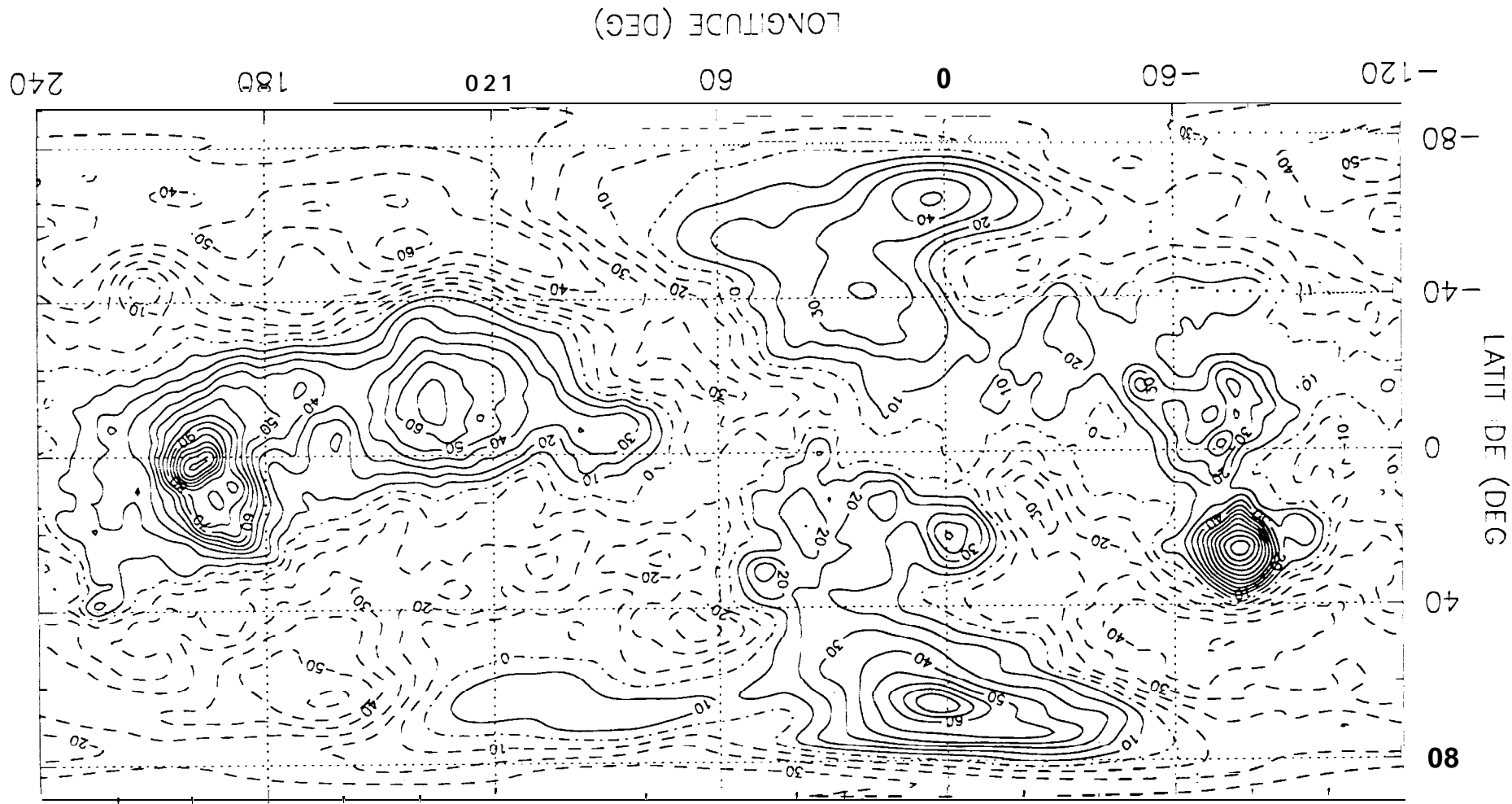


Figure 3
 Nonopliv

Figure 3
 Nonopliv

Figure 4
Moscow

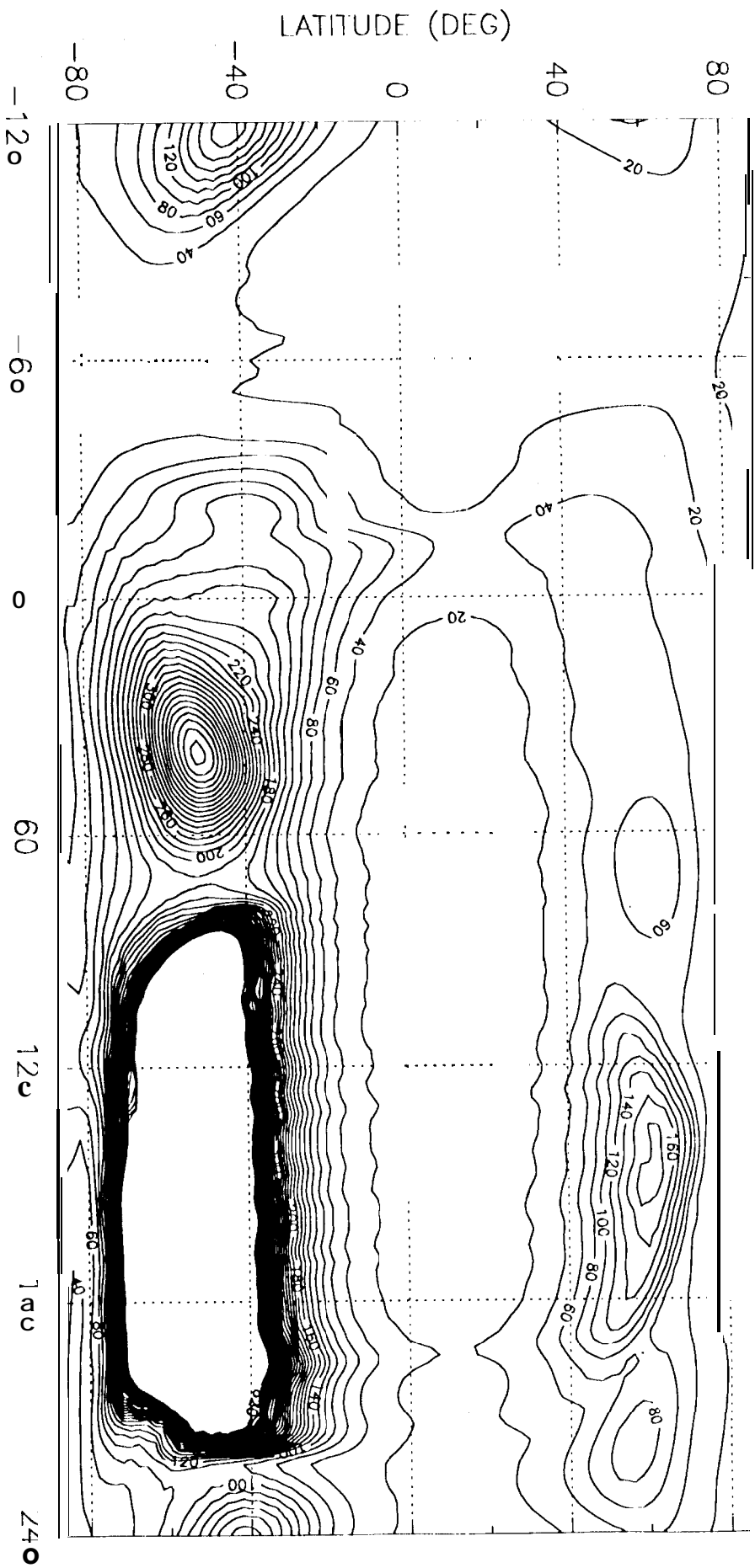


Figure 4
Konoplin

Figure 5
Konoplin

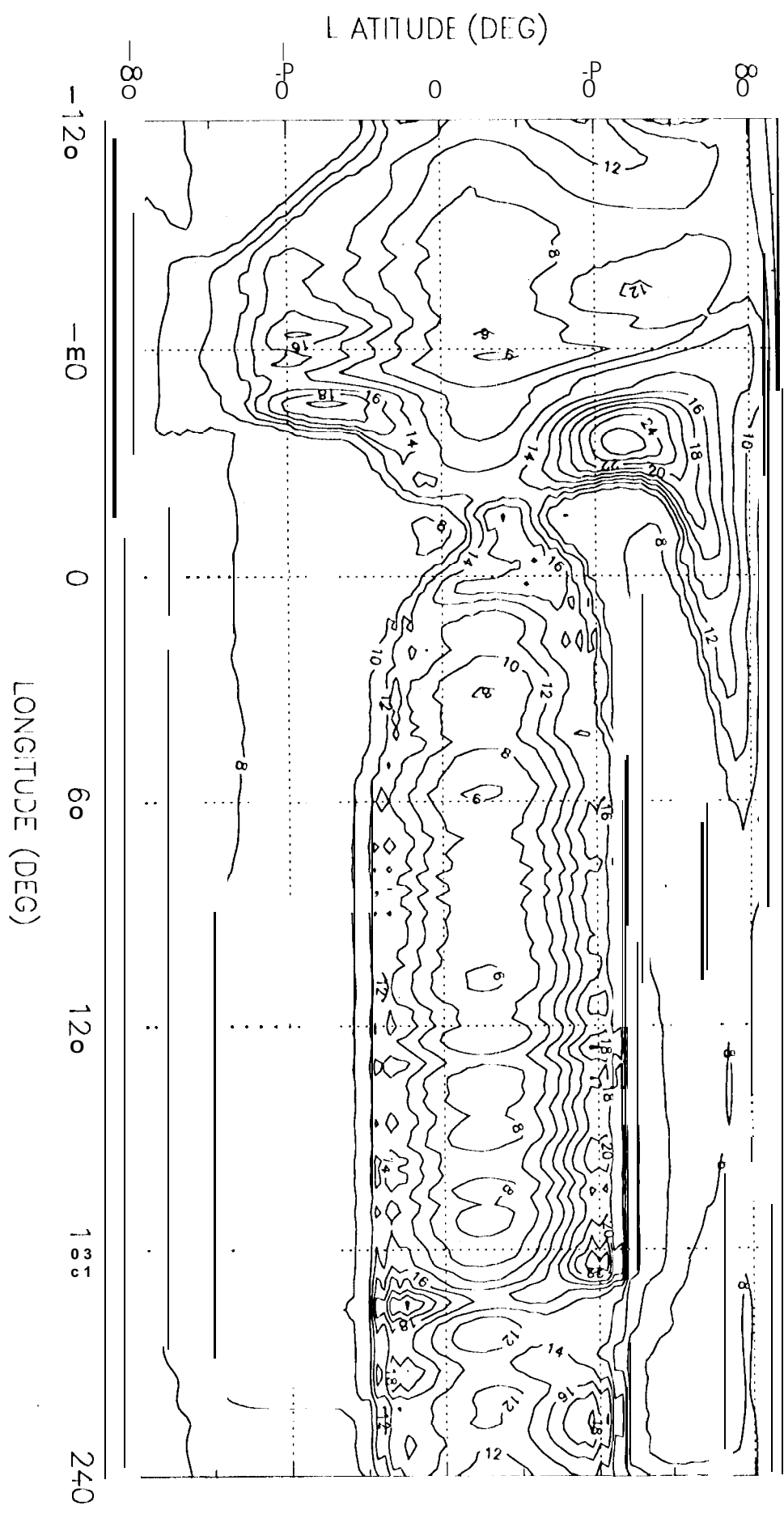


Figure 5
Konoplin

Figure 6
Konopliv

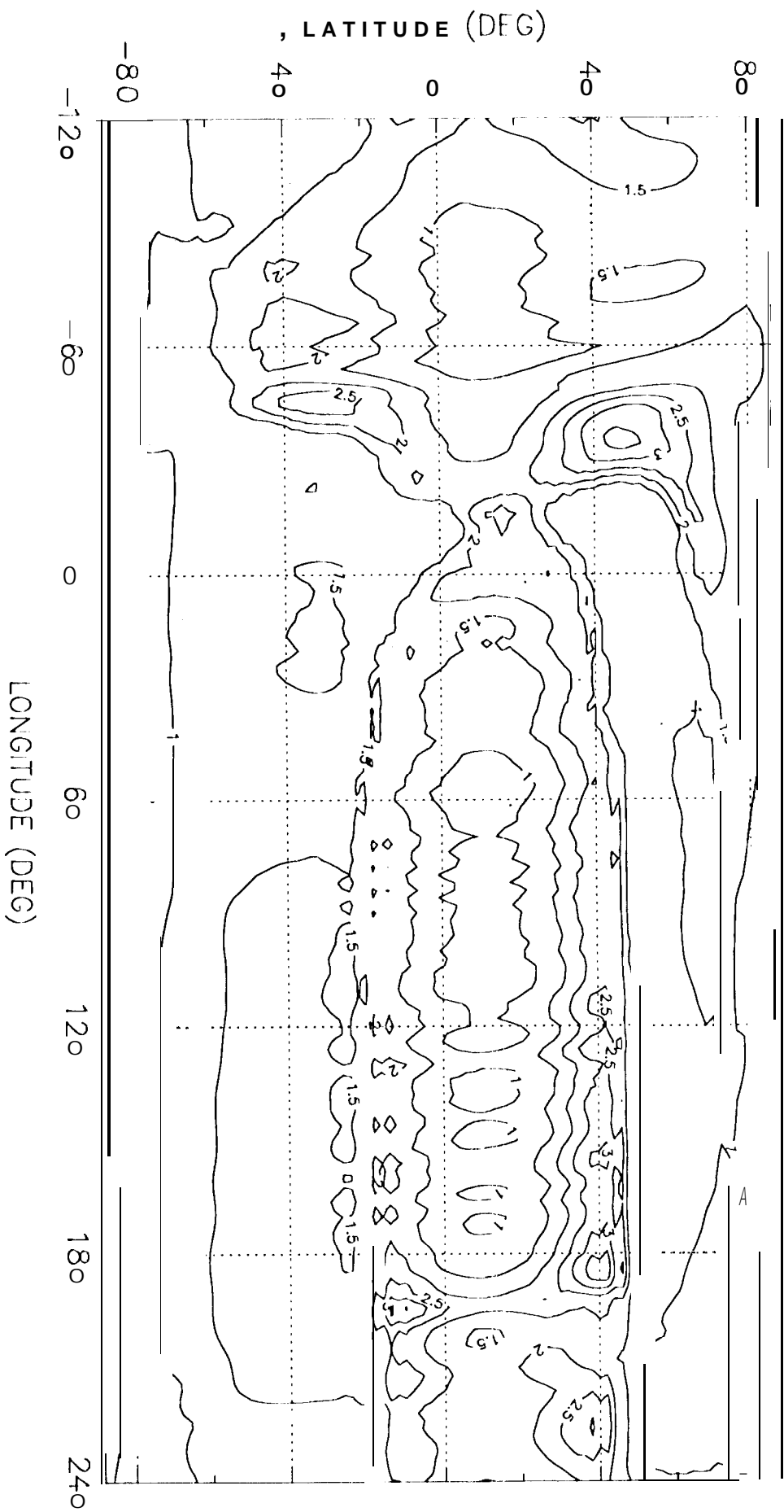


Figure 6
Konopliv

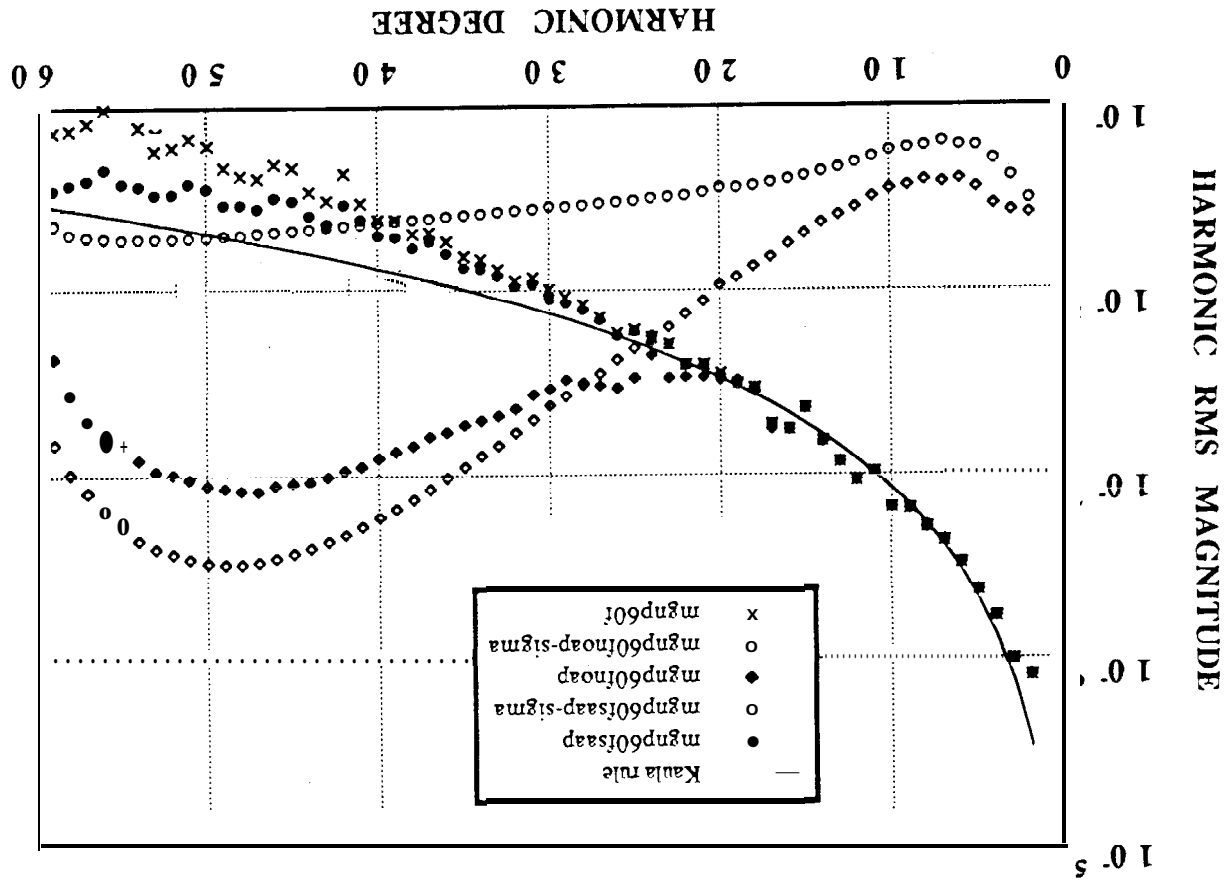


Figure 7
Konopliv

Figure 7
Konopliv

Figure 2
Konopliv

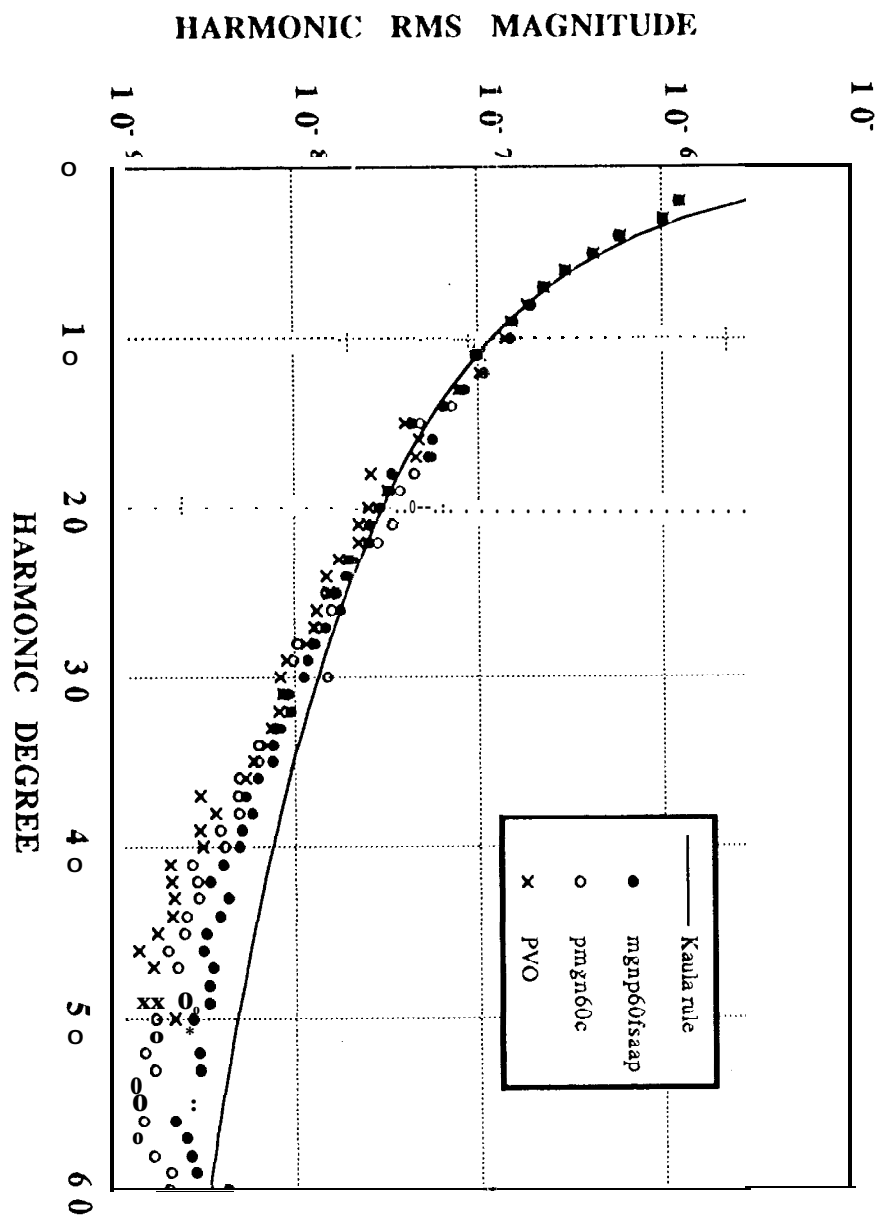


Figure 3
Konopliv

Figure 9
Konoplin

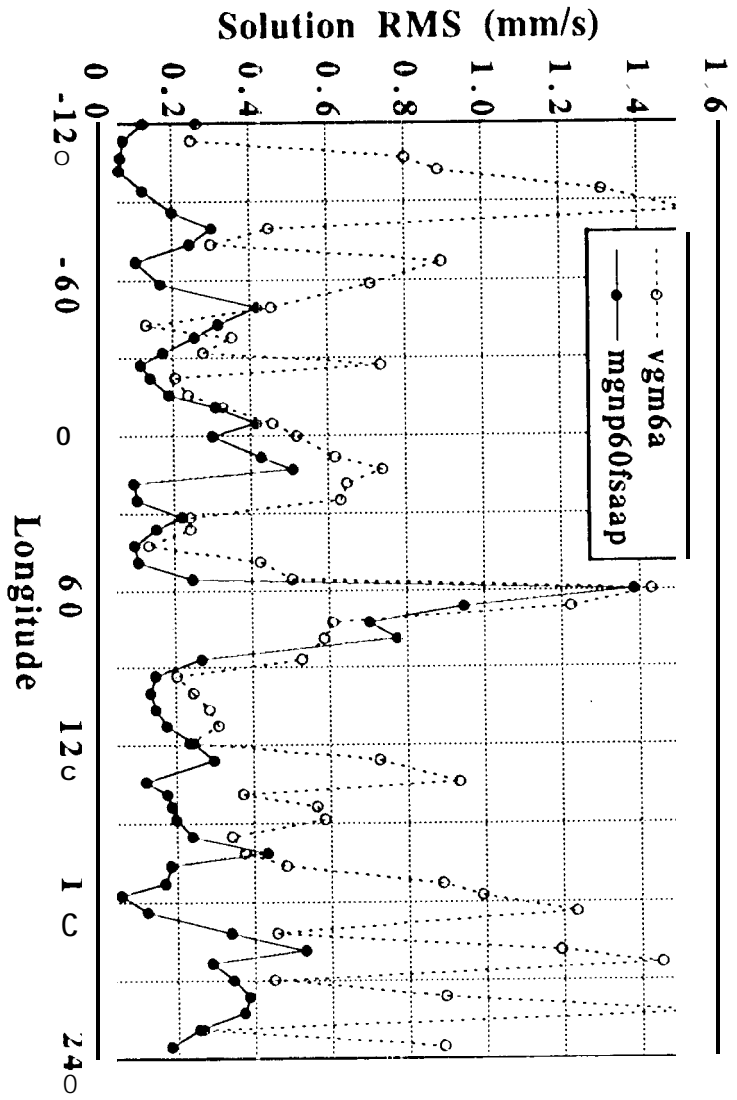


Figure 9
Konoplin

Figure 10
Korepfin

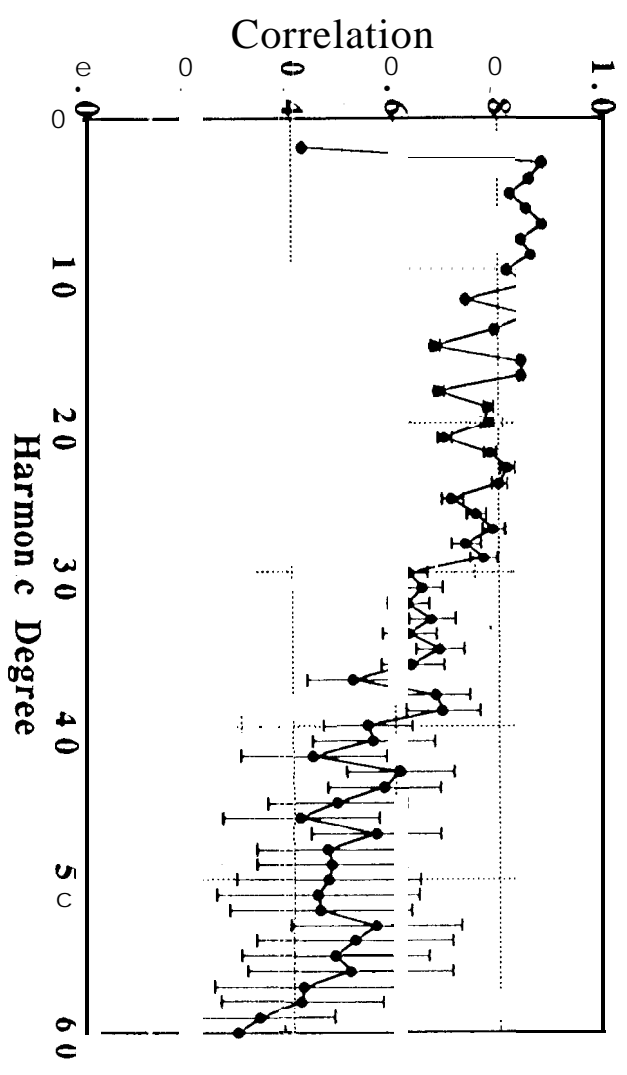


Figure 10
Korepfin

Figure 11
Konoplin

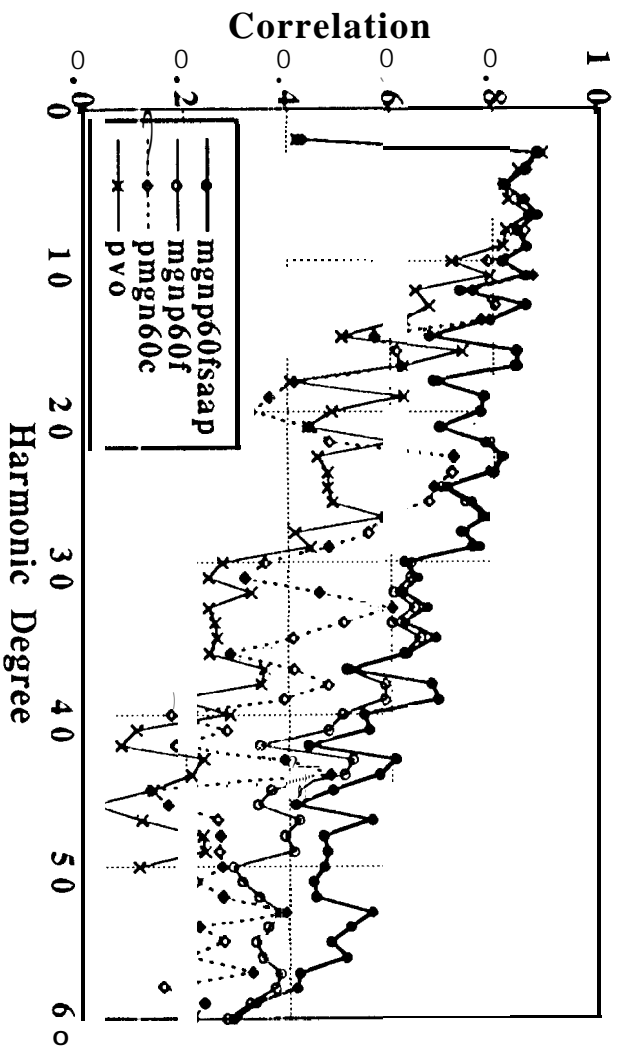


Figure 11
Konoplin

Figure 12
Konoplin

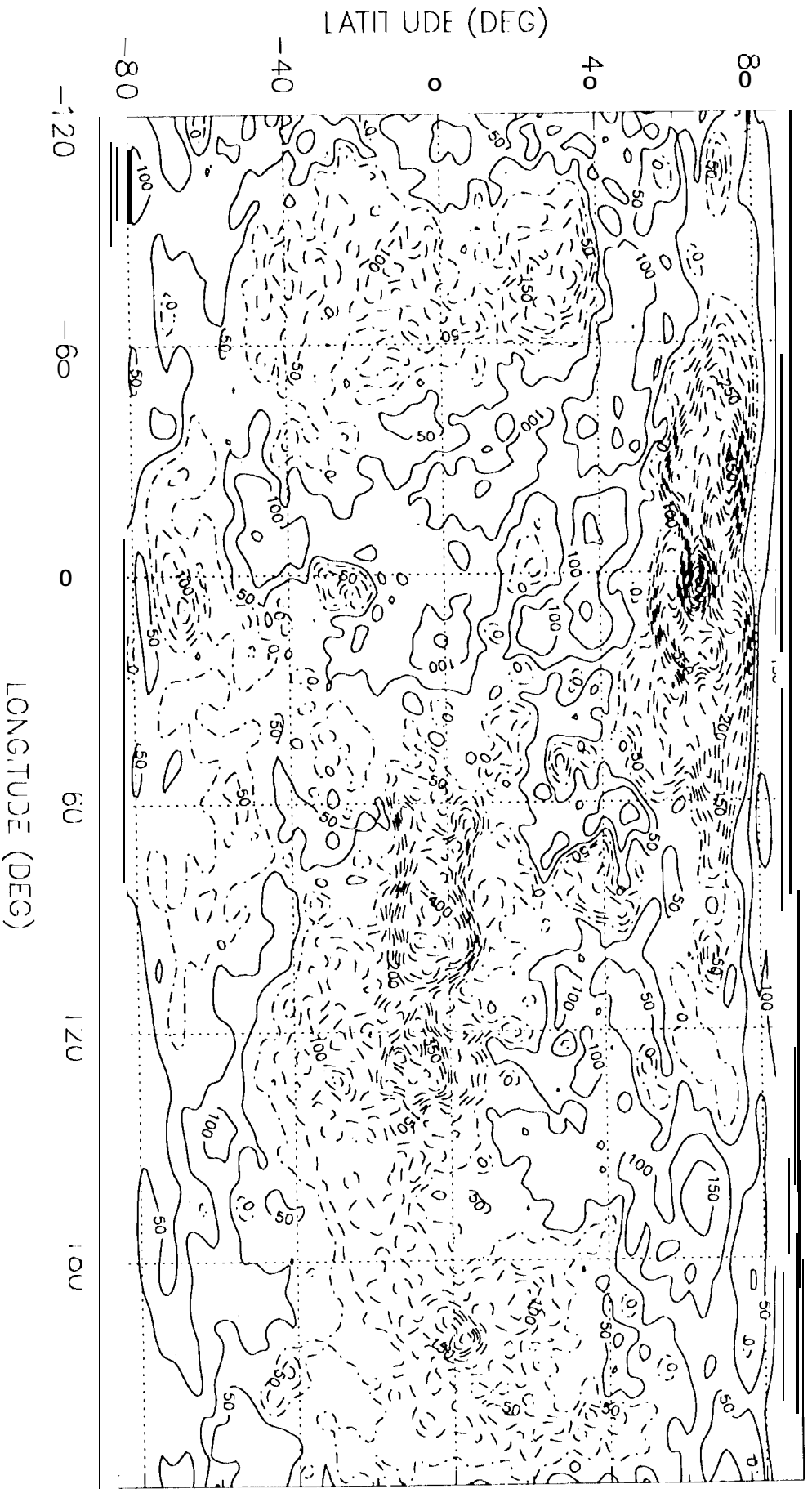


Figure 12
Konoplin

Figure 13
Konoplin

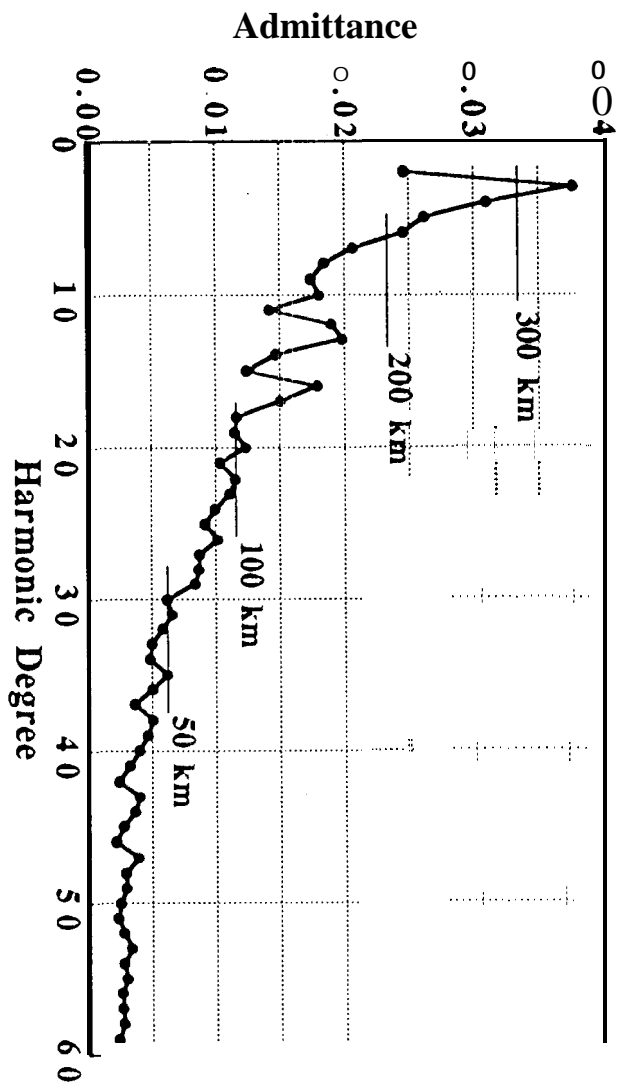


Figure 13
Konoplin

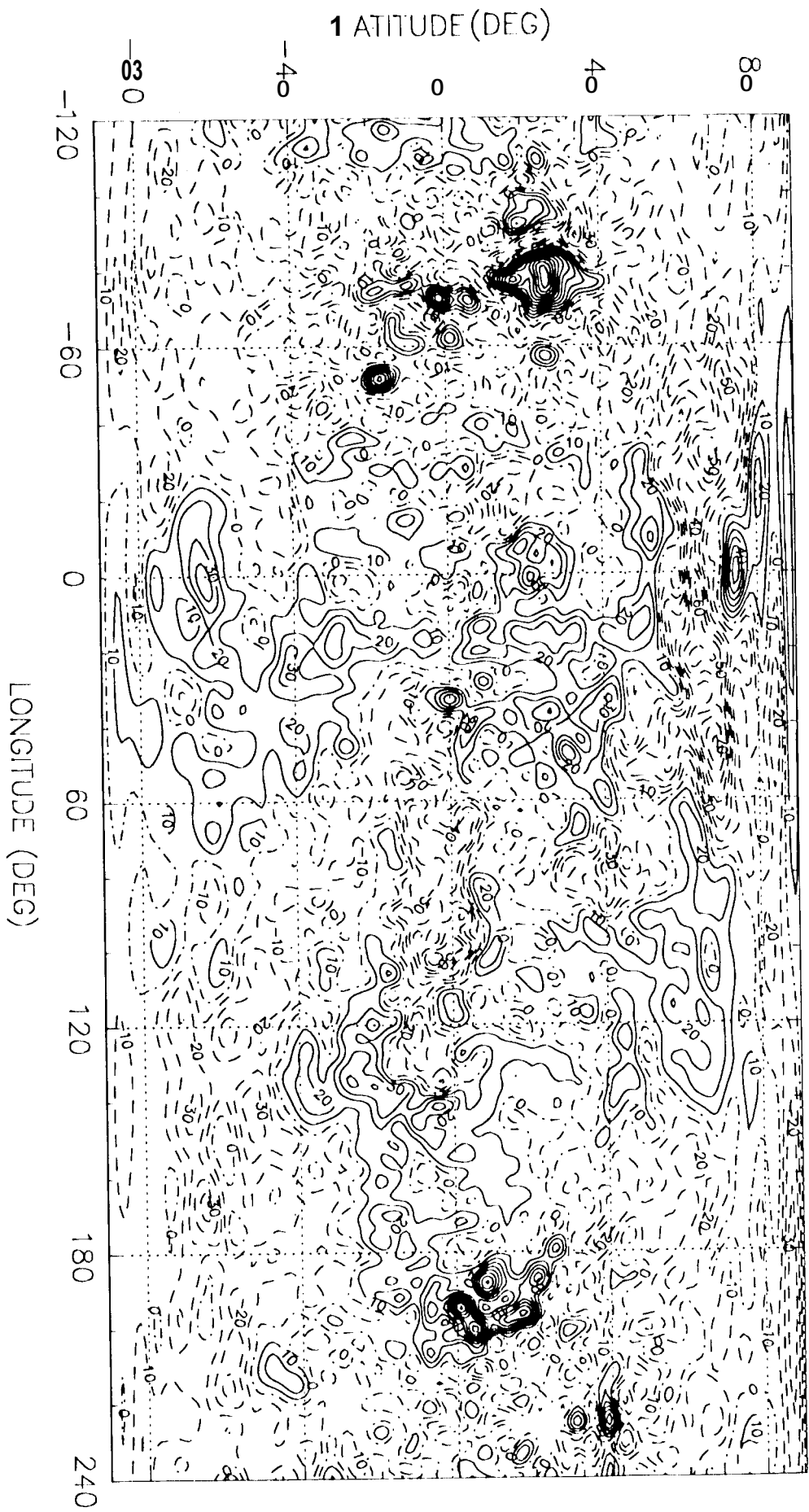


Figure 14
Konoplin

Figure 15
Konoplin